INTERNATIONAL JOURNAL OF HYDROGEN ENERGY 46 (2021) 40175–40184

Available online at www.sciencedirect.com

ScienceDirect

journal homepage: www.elsevier.com/locate/he

# Hydrogen effect on phase angle shift in electrochemical impedance spectroscopy during corrosion fatigue crack emanation

*Xiankang Zhong* [a], *Yuantai He* [a], *Noam Eliaz* [b], *Kyra Sedransk Campbell* [c], *Junying Hu* [a,*]

[a] *State Key Laboratory of Oil and Gas Reservoir Geology and Exploitation, Southwest Petroleum University, Chengdu 610500, China*

[b] *Department of Materials Science and Engineering, Tel-Aviv University, Ramat Aviv, Tel Aviv 6997801, Israel*

[c] *Department of Chemical and Biological Engineering, University of Sheffield, Mappin Street, Sheffield, S1 3DJ, UK*

## HIGHLIGHTS

- Hydrogen leads to a lower peak intensity and shifts the peak to a higher frequency.
- Hydrogen causes the formation of a crack with shorter length than its absence.
- Hydrogen results in shortening crack initiation time and corrosion fatigue life.

## ARTICLE INFO

*Article history:*
Received 9 July 2021
Received in revised form
15 September 2021
Accepted 24 September 2021
Available online 12 October 2021

*Keywords:*
Corrosion fatigue
Hydrogen
Phase angle
Crack formation

## ABSTRACT

It is generally considered that hydrogen could accelerate the corrosion fatigue process, however, the effective monitoring approach for the corrosion fatigue development in the hydrogen related environment is still missing. In this work, the hydrogen effect on phase angle shifts in electrochemical impedance spectroscopy during corrosion fatigue crack formation in drill pipe steel was *in-situ* studied. The results show that phase angle shifts as a function of time could be used to monitor the corrosion fatigue development in the presence of hydrogen. The permeated hydrogen leads to a lower peak intensity and shifts the peak to a higher frequency on the phase angle *vs.* frequency curve. These differences are due to the formation of a corrosion fatigue crack with a shorter length than in the absence of hydrogen. The phase angle shift reveals that the presence of hydrogen results in shortening crack initiation time and corrosion fatigue life of the drill pipe steel.

© 2021 Hydrogen Energy Publications LLC. Published by Elsevier Ltd. All rights reserved.

## Introduction

Drilling tools, critical components in the exploitation process for recovering oil and gas, encounter a range of challenging environments during their operation [1–5]. In particular, the drill pipe is a critical component in the drill string which must not only withstand complicated alternating loads; but also, it must serve as a channel to circulate drilling fluid in which corrosive species are usually present [6,7]. Due to these

* *Corresponding author.*
E-mail address: hujunying01@yeah.net (J. Hu).

https://doi.org/10.1016/j.ijhydene.2021.09.205

0360-3199/© 2021 Hydrogen Energy Publications LLC. Published by Elsevier Ltd. All rights reserved.

combined effect of the alternating loads and the corrosive environment, corrosion fatigue failures of drill pipes occur frequently.

Sour drilling environments contain gaseous or liquid hydrogen sulfide ($H_2S$), further increasing the risk of hydrogen embrittlement and failure of drill pipes. When most of carbon steels are exposed to the wet $H_2S$-containing environment, hydrogen atoms can easily penetrate into the bulk steel, subsequently leading to hydrogen blistering or hydrogen-induced cracking phenomena [8–16]. In addition, under the combined effect of loads and hydrogen, catastrophic drill pipe corrosion fatigue failures have been reported to occur [17,18]. Li et al. [19] studied the fatigue and corrosion fatigue behaviors of G105 and S135 steels in $H_2S$-containing environment, respectively. It was found that there was no obvious fatigue limit for these steels in $H_2S$-containing solutions; further, it was demonstrated that the fatigue cracks initiated from the surface and then propagated continuously into the bulk material. Liu et al. [20] discussed the corrosion fatigue propagation behavior of S135 steel drill pipe in $H_2S$-containing environment. It was shown that $H_2S$ caused a distinct acceleration of the corrosion fatigue crack propagation rate; the propagation rate in $H_2S$-containing solution was about ten times higher than that in a $H_2S$-free environment. Investigations of the mechanical and corrosion properties of drill pipe steel charged electrochemically with hydrogen [21–23] have indicated that the introduction of hydrogen not only deteriorated the mechanical properties, but also made the drill pipe more susceptible to corrosion.

According to the literature [17–20,24–27], the presence of hydrogen both accelerates corrosion and increases the risk of fatigue of the steels in the operation environment. Therefore, it can be expected that corrosion fatigue would also accelerate in the presence of hydrogen. Unfortunately, existing literature investigating *in situ* analysis of corrosion fatigue of steels, in the presence of hydrogen, is insufficient. Furthermore, the monitoring of corrosion fatigue crack formation under such environment remains unreported.

Bosch et al. [28,29] and Luo et al. [30] reported an *in situ* method for monitoring the initiation and propagation of stress corrosion cracking (SCC) by electrochemical impedance spectroscopy (EIS). They observed that crack formation caused changes in the EIS phase angle. Previously, we also developed a new experimental methodology and apparatus where a fatigue test and EIS measurement could be carried out at the same time [31]. This novel approach demonstrated that the correlation between the length of corrosion fatigue crack and phase angle shift could be studied; furthermore, it was demonstrated that phase angle shift could be employed to reveal the crack initiation and propagation in corrosion fatigue test. As such, we anticipate that EIS phase angle data can also be employed to reveal the corrosion fatigue crack formation in the presence of hydrogen.

Due to the toxicity of $H_2S$ and the compounding dangers in employing a rotating fatigue test, in the presence of $H_2S$, a common proxy experiment was employed: electrochemical hydrogenation. In this technique, electrochemical hydrogen-charging introduces hydrogen into the steel substrate, providing improved safety whilst being both cost efficient and simple to execute [32,33].

The objective of this work is to unmask the hydrogen effect on the phase angle shifts of electrochemical impedance spectroscopy of drill pipe steel in the presence of hydrogen.

## Experimental

G105 drill pipe steel, a material commonly used for drill pipe in oil and gas fields where $H_2S$ exists [34], was used in this work. The chemical composition (wt. %) of the G105 drill pipe steel is as follows: C 0.26, Si 0.26, Mn 1.08, P 0.09, S 0.04, Cr 0.83, Mo 0.17, Ni 0.04, Ti 0.02, with Fe as balance. The C and S contents were measured using a Carbon–Sulfur Analyzer instrument (a CS-3000 system, NCS Testing Technology Co. Ltd., China), while the other elements were measured by Atomic Absorption Spectroscopy (iCE 300, Thermo Fisher Scientific, MA, USA). In the corrosion fatigue experiments, a standard fatigue sample was machined from a drill pipe, as schematically illustrated in Fig. 1a.

3.5 wt% NaCl solution was employed as the test solution, which was prepared from NaCl and deionized water (DI water). The solution used for hydrogenation was 0.2 mol/L sulfuric acid ($H_2SO_4$) with the addition of 1 g/L thiourea ($CH_4N_2S$). The latter was added as a surface poison in order to prevent hydrogen atoms from recombination [35,36].

The solution was deaerated with $N_2$ gas for 2 h before the onset of hydrogenation, and $N_2$ purging continued throughout the experiment. Hydrogenation was done using a two-electrode setup where the G105 steel sample and a Pt sheet were the working electrode (WE) and counter electrode (CE), respectively. The exposed surface area of the G105 steel sample was 2.5 $cm^2$. The phase shift is determined by the ratio between the surface area of the electrode and the surface area of the crack, i.e., the phase shift in EIS decreases with increasing surface area or sample diameter. The details can be found in the previous literature [28]. This is why the surface area of the sample is required to be controlled. The current density was maintained at $-20$ mA/$cm^2$ during the whole hydrogenation period (12 h). Following hydrogenation, the sample was immediately rinsed with deionized (DI) water and ethanol, and subsequently dried in a $N_2$ gas flow. Then, it was used immediately in the corrosion fatigue experiment.

In our previous work [31], an experimental setup for real-time monitoring of the electrochemical parameters during corrosion fatigue experiments was developed. This setup is composed of a pure bending fatigue testing machine and a cell for electrochemical measurement (Fig. 1b). Detailed information can be found elsewhere [31].

EIS measurements were conducted periodically (one measurement every 30 min) during the corrosion fatigue test, employing a standard three-electrode setup. The corrosion fatigue sample was employed as a WE, a coiled Pt wire was as a CE, and Ag/AgCl (satd. KCl) electrode was used as a reference electrode. In order to ensure identical exposed surface area in all experiments, silicone sealant was employed to mask untested area on the WE (Fig. 1c). The sample was rotated in the test solution at a speed of 40 cycles/min, and the stress was kept constant at 176 MPa. EIS measurements were performed using a CS 350 electrochemical workstation (Wuhan Corrtest Instruments Corp. Ltd., China). A sinusoidal potential

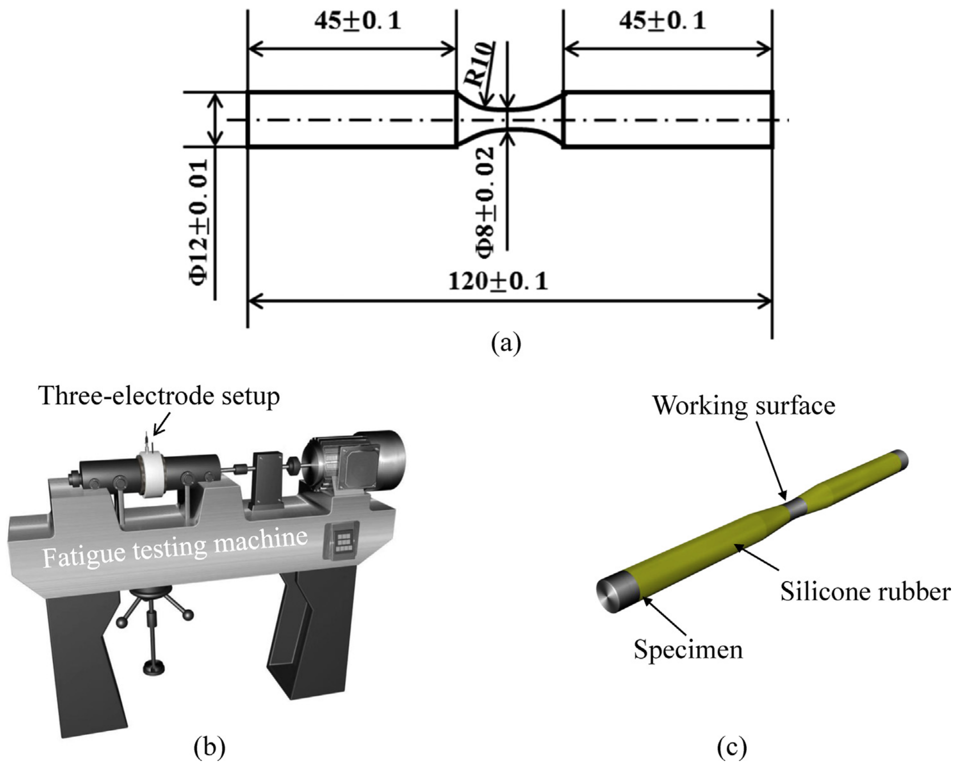


**Fig. 1 – (a) Schematics of (a) corrosion fatigue sample (dimensions in mm), (b) corrosion fatigue test setup, and (c) the G105 sample used for corrosion fatigue experiments.**

perturbation of 10 mV was used during the EIS measurement and the frequency range was: 100 kHz to 10 mHz. Throughout the experiment, the temperature inside the cell was maintained at 25 ± 0.5 °C.

The fracture morphologies of samples with or without hydrogen were characterized using a FEI Quanta 450FEG scanning electron microscope (SEM, Oregon, USA). Cross-sections were inspected by a digital camera (PowerShot SX, Canon Inc., Tokyo, Japan).

## Results and discussion

### *The phase angle characteristics in the presence vs. in the absence of hydrogen*

It has been reported that the phase angle shift in the specific frequency range could be used to monitor crack formation in SCC [28–30]. In order to establish how the corrosion fatigue crack impacts the phase angle in the presence of hydrogen, phase angle of the sample at each frequency was first measured at the beginning and at the end of fatigue test. At the beginning of the experiment, no crack is present on the sample surface. Therefore, the curve measured at the beginning of the experiment is labelled "without crack" (Fig. 2a). As the experiment proceeds, cracks will initiate and propagate. Accordingly, it is certain that crack is present on the sample at the end of the fatigue test and the curve recorded at the end of the experiment is labelled "with crack" (Fig. 2a).

From Fig. 2a, it is evident that the curves of cracked and uncracked sample are distinct from one another, for the uncharged sample. The curve before cracking on the sample has occurred shows a maximum at 4.3 Hz and ca. −56.4°. After the sample has cracked there is also a maximum in the phase angle *vs.* frequency curve; however, it appears at 0.2 Hz and ca. −31.9°. The presence of a crack results in shift of the phase angle peak to a lower frequency and with a reduced intensity (*i.e.* in the less negative direction). These results are in consistent with those of artificial crack experiments in our previous work [31].

The phase angle vs. frequency curves of the hydrogenated samples, in 3.5 wt% solution, taken before and after the formation of a crack, *i.e.* with or without a crack, are shown in Fig. 2b. The experiment taken before the crack (without crack) has a peak maximum on the curve at 14.5 Hz and *ca.* −60.1°. After the formation of the crack, the peak maximum is shifted to 4.3 Hz and *ca.* −45.8°. The relationship between the pre- and post-crack measurements (namely peak maximum phase angle and intensity changes) are consistent between the uncharged and charged samples; *i.e.*, the presence of a crack shifts the EIS phase angle peak to both lower frequency and lower intensity.

In principle, inherent variation in phase angle for the same sample (*i.e.*, either the hydrogenated or non-hydrogenated one presented herein) is possible; this includes attributions to either change in surface condition or crack formation. To rule out the possible influence of the surface condition, a parameter Δ*p*, was defined to equal the change in phase angle

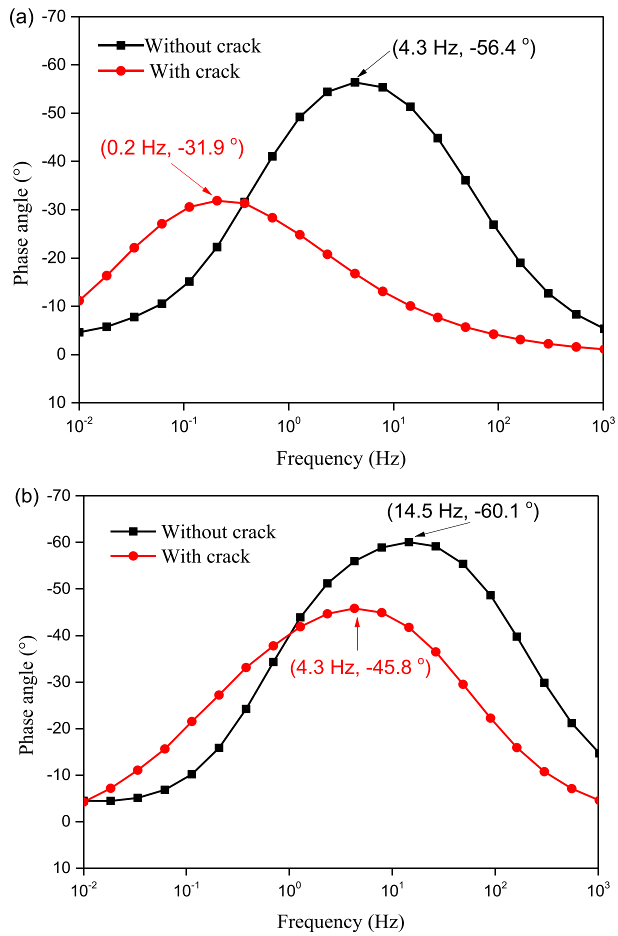


**Fig. 2 – The phase angle vs. frequency curves of samples in 3.5 wt% NaCl solution both with or without crack: (a) uncharged sample and (b) hydrogenated sample.**

at the same frequency between the same sample either cracked or uncracked, as expressed by Eq. (1):

$$\Delta p = p_{uc} - p_c \tag{1}$$

In which $p_{uc}$ represents the phase angle of uncracked sample and $p_c$ is the phase angle of cracked sample. During the experiment, the EIS of a sample in 3.5 wt% NaCl solution was first measured. Then, the same sample was carefully cleaned and used it to run the fatigue test in the air. Once the fatigue test was ended, the cracked sample was obtained. Subsequently, the EIS of this cracked sample was measured in 3.5 wt% NaCl solution. In this case, $\Delta p$ can be obtained based on Eq. (1). Employing $\Delta p$ will ensure that only changes in phase angle resulting from crack formation are revealed.

The previously presented comparison between the uncharged and hydrogenated samples are presented in Fig. 3 as $\Delta p$ vs. frequency. The normalized employed supports the previously suggested findings above that the presence of hydrogen decreases the differences in phase angle between cracked and uncracked samples, and the maximum value of $\Delta p$ also shifts to higher frequency. The reason for the effect of hydrogen on $\Delta p$ will be explored in Section Theoretical explanation of the phase angle shift in the presence of hydrogen.

### *Theoretical explanation of the phase angle shift in the presence of hydrogen*

The phase angle are affected by both the surface condition of the sample and the crack impedance [31]. Therefore, the impedance of the sample with and without a crack may be represented by the equivalent circuits shown in Fig. 4.

The representations presented in Fig. 4a and b for the impedance under the two scenarios of interest, are expressed mathematically, where $Z_{woc}$ is the impedance without a crack present (Eq. (2)) and $Z_{wc}$ is with a crack present (Eq. (3))

$$Z_{woc} = \frac{R_{surf}}{1 + R_{surf}Q_{surf}(j\omega)^{n_{surf}}} + R_S \tag{2}$$

$$Z_{wc} = \frac{R_{surf}Z_{crack}}{R_{surf} + Z_{crack} + Q_{surf}(j\omega)^{n_{surf}}Z_{crack}} + R_S \tag{3}$$

where the terms employed are consistent with Fig. 4. Additional terms are: $j$ is the imaginary unit, $n_{surf}$ is the dispersion index, and $\omega$ is the angular frequency. The term $Z_{crack}$ will be further explored as it is a complex variable here which is composed of various other factors. Regardless, the difference between the impedance of the system with and without a crack is expressed as:

$$\Delta Z = Z_{wc} - Z_{woc} \tag{4}$$

In its simplest form, $Z_{crack}$ has been described as the impedance of a round hole. This has been previously employed in a model (Bosch et al. [28]) where a crack impedance model of SCC was suggested to consist of round-hole-cracks. The impedance of a round-hole-crack ($Z_{crack}$) is a function of crack-tip impedance ($Z_{cracktip}$), crack-wall impedance per unit length ($Z_{wall}$), the resistance of solution inside the round crack per unit length ($R_{sol}$), and the round-crack length ($L$). Therefore, $Z_{crack}$ can be described as Eq. (5) [29]. This model starts with the transmission line model, used for the cylindrical pore model to describe the impedance of porous electrodes, the details can be found in previous work [29].

$$Z_{crack} = \frac{\sqrt{R_{sol}Z_{wall}}}{Z_{cracktip}}\left(1 + \frac{Z_{cracktip} - \frac{\sqrt{R_{sol}Z_{wall}}}{Z_{cracktip}}}{\frac{\sqrt{R_{sol}Z_{wall}}}{Z_{cracktip}} + \frac{1}{\coth\left(L\sqrt{\frac{R_{sol}}{Z_{wall}}}\right)}}\right) \tag{5}$$

A corrosion fatigue crack can also consist of a finite number ($m$) of round holes with the same length [31]. In this scenario, to take the frequency dispersion into consideration, the dispersion index ($n$) is introduced into the corrosion fatigue crack-tip impedance and the corrosion fatigue crack-wall impedance, *i.e.*, the capacitance of the electrical double layer is replaced by a CPE.

Therefore, $Z_{cracktip}$ is defined as a function of crack-tip resistance ($R_{cracktip}$) and the double-layer capacitance at the crack tip ($Q_{cracktip}$), which can be regarded as a prefactor of a

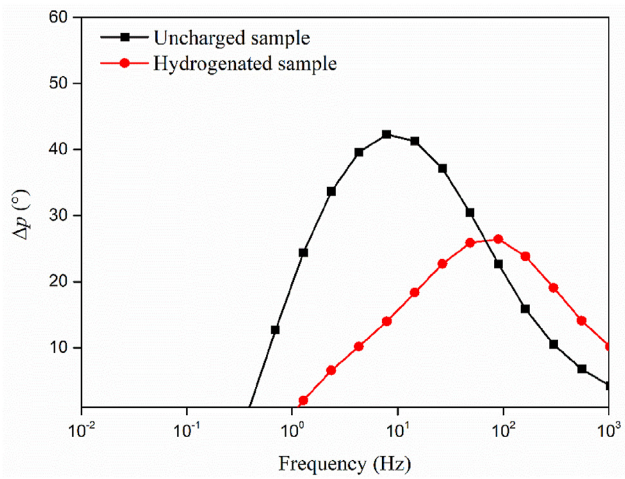


**Fig. 3 – Δp vs. frequency curves of both uncharged and hydrogenated samples in 3.5 wt% NaCl solution.**

CPE. Similarly, $Z_{wall}$ is related to $R_{wall}$ and $Q_{wall}$. Therefore, $Z_{cracktip}$ and $Z_{wall}$ can be described as follows:

$$Z_{cracktip} = \frac{R_{cracktip}}{1 + R_{cracktip}Q_{cracktip}(j\omega)^{n_{cracktip}}} \quad (6)$$

$$Z_{wall} = \frac{R_{wall}}{1 + R_{wall}Q_{wall}(j\omega)^{n_{wall}}} \quad (7)$$

Combining Eqs. (2)–(7), the difference in impedance of the sample, either cracked or uncracked, is as follows:

$$\Delta p = \tan^{-1}\left(\frac{\Delta Z_{im}}{\Delta Z_{re}}\right) \quad (9)$$

Once a corrosion fatigue crack emanates from the surface to the bulk steel, the parameters $R_{surf}$, $Q_{surf}$, $R_{sol}$, $R_{wall}$, $R_{cracktip}$, $Q_{wall}$ and $Q_{cracktip}$ will be fixed during the experiment. According to Eq. (8), the parameter $\Delta p$ is determined by the crack length $L$ at a certain angular frequency $\omega$.

In order to understand the relationship between $\Delta p$ and $L$ at each frequency more directly, three exemplar crack lengths ($L$ = 1, 1.5 and 2 mm) were studied (Fig. 5). The parameters required to calculate $\Delta p$ at each condition are listed in Table 1. As the crack length increases, the entirely of the peak, as well as the maximum comparatively shifts to lower frequencies. Additionally, as the crack length increases the intensity increases, although less significantly from 1 to 1.5 mm crack length. The relationship can be considered in the context of the previously presented experimental results (Fig. 3). In the presence of hydrogen, the peak intensity of $\Delta p$ is lower than that in the absence of hydrogen, whilst the frequency of the peak is higher than its counterpart. As such, this implies that the length of the crack formed on the sample in the presence of hydrogen is shorter than that without hydrogen. This is confirmed by optical cross-section macrographs of cracks formed on hydrogenated and uncharged samples (Fig. 6). It is apparent that the length of the crack formed in the hydrogenated sample is much shorter than that in the uncharged sample.

The fracture morphologies of the uncharged and hydrogenated samples are shown in Fig. 7. The uncharged sample

$$\Delta Z = \frac{-mR_{surf}^2}{1 + Q_{surf}(jw)^n} \times \frac{1 + \sqrt{R_{sol}Z_{wall}}\coth\left(L\sqrt{\frac{R_{sol}}{Z_{wall}}}\right)}{\left(1 + Q_{surf}(jw)^n\right)\sqrt{R_{sol}Z_{wall}} + mR_{surf}Z_{cracktip} + \left(mR_{surf}\sqrt{R_{sol}Z_{wall}} + \left(1 + Q_{surf}(jw)^n\right)Z_{cracktip}\sqrt{R_{sol}Z_{wall}}\right)\coth\left(L\sqrt{\frac{R_{sol}}{Z_{wall}}}\right)} \quad (8)$$

Accordingly, $\Delta p$ can be described as follows:

experienced a ductile fracture, as is evident by the presence of many dimples on the fracture surface. By contrast, the

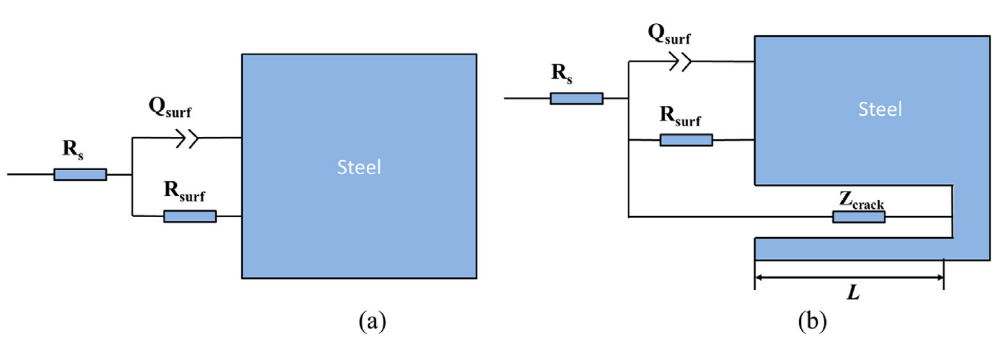


**Fig. 4 – Equivalent circuit models for the impedance before cracking (a) and after cracking (b) samples. In both circuits $R_s$ is the solution resistance, $R_{surf}$ represents the surface resistance of WE, $Q_{surf}$ is the capacitance of a constant phase element (CPE) of the WE surface, $Z_{crack}$ is the impedance of the crack, and $L$ stands for the length of the crack.**

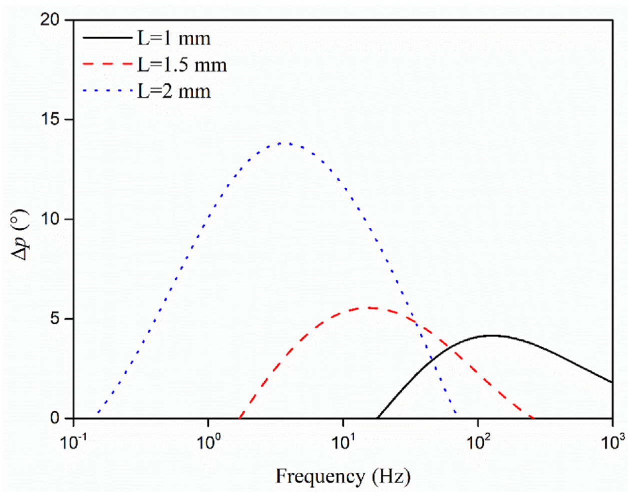


**Fig. 5 – The calculated $\Delta p$ (From Eq. (8)) vs. frequency curves generated for the same sample with different crack lengths, where three lengths are considered: 1, 1.5 and 2 mm.**

hydrogenated sample exhibits brittle fracture characteristics, namely cleavage fracture. These visual indicators of different failure mechanisms indicate that hydrogen decreases the toughness of the drill steel. The implication of this change to the steel itself is that the corrosion fatigue life is likely shortened.

The fracture morphology of each sample is composed of three zones: crack initiation, crack propagation, and final fracture. In the crack initiation zone, some pits (not shown herein) were noticed, which probably served as initiation sites for the fatigue crack. The crack propagation zone of the uncharged sample is remarkably larger than that of the hydrogenated sample. This means that the crack length in the uncharged sample is longer than that in the hydrogenated sample. These results also support our aforementioned conclusion that hydrogen decreases the crack length, hence the smaller $\Delta p$, lower peak intensity and its shift to higher frequency.

### *Monitoring the corrosion crack formation in the presence and absence of hydrogen*

The presence of hydrogen has been suggested results in a crack with a shorter length than in the absence of hydrogen. However, this phenomenon does not explain how hydrogen affects the corrosion fatigue life and corrosion fatigue crack initiation time. In order to better understand these, the phase angle shift was used to reveal the initiation and propagation of a corrosion fatigue crack in the presence and absence of hydrogen.

As previously described in Section The phase angle characteristics in the presence vs. in the absence of hydrogen, the observed variation in phase angle can be attributed to two factors: change in surface condition and crack formation.

In order to accurately monitor crack initiation and propagation using phase angle shift, the contribution of variation in surface condition to the phase angle shift over time should be ruled out. To achieve this, a matrix of four experiments were deployed considering combinations with and without hydrogen, and with and without loading. Without loading, no crack will form. Therefore, the change in phase angle is only resulted from the surface condition variation, *e.g.* due to corrosion. However, when load is applied, the phase angle shift can be affected by both surface condition and crack formation. Therefore, we use the term "*phase shift angle*" to represent the difference between the phase angle of a loaded sample as compared to the phase angle of an unloaded sample in the test solution in both cases. Namely, we first measured the EIS very 10 min of a loaded sample in 3.5 wt% NaCl solution during the fatigue test. This periodical measurement did not stop until the end of the fatigue test. Then, we measured the EIS very 10 min of an unloaded sample 3.5 wt% NaCl solution. The total test time for the unloaded sample was the same with the case of loaded sample. Finally, we could get the *phase shift angle vs. time* curve at each frequency. It should be noted that the effect of the load on the change in surface condition is neglected.

The phase shift angle vs. time curves of both hydrogenated and uncharged samples are presented in Figs. 8 and 9,

**Table 1 – Selected parameters for plotting of Fig. 5 [31].**

| Parameter | Value |
|---|---|
| Crack-tip resistance, $R_{tip}$ | 24 kΩ |
| Crack-wall resistance per unit length, $R_{wall}$ | 10 kΩ mm |
| Solution resistance inside crack, $R_{sol}$ | 1.8 kΩ/mm |
| Constant phase angle component of crack wall per length, $Q_{wall}$ | 39.449 μF/mm |
| $n_{wall}$ | 0.76 ($L = 1$ mm), 0.63 ($L = 1.5$ mm), 0.72 ($L = 2$ mm) |
| Constant phase angle component of crack tip, $Q_{tip}$ | $39.032 \times 10^{-6}$ 1/(Ω cm$^2$ s$^n$) |
| $n_{tip}$ | 0.76 ($L = 1$ mm), 0.63 ($L = 1.5$ mm), 0.72 ($L = 2$ mm) |
| Solution resistance, $R_S$ | 14.17 Ω |
| Surface resistance, $R_{surf}$ | 271 Ω |
| Surface constant phase angle component, $Q_{surf}$ | 839.37 1/(Ω cm$^2$ s$^n$) |
| $n_{surf}$ | 0.76 |
| The number of round hole cracks, $m$ | 2 |
| Crack length, $L$ | 1, 1.5, 2 mm |
| Crack width, $d$ | 0.5 mm |

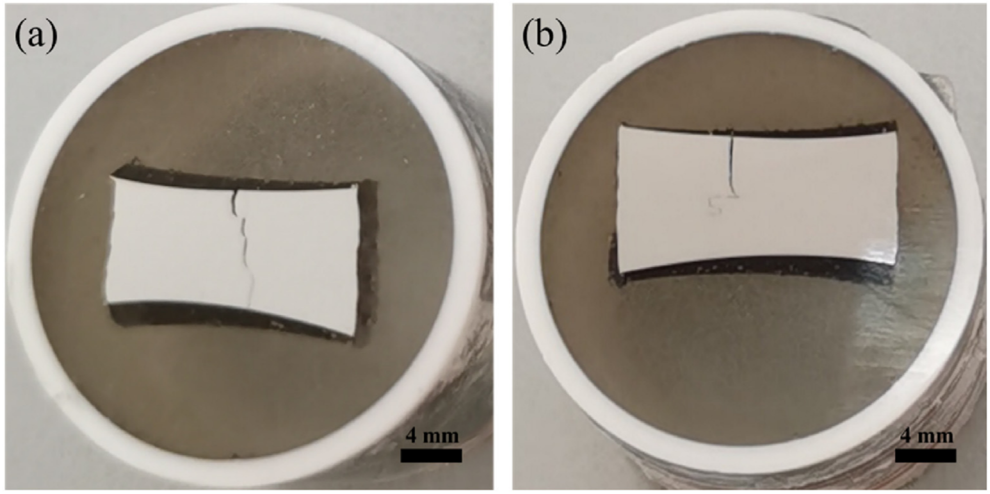


**Fig. 6 – Cross-section optical macrographs revealing the cracks formed on (a) uncharged sample, and (b) hydrogenated sample after corrosion fatigue tests in 3.5 wt% NaCl solution under an applied stress of 176 MPa.**

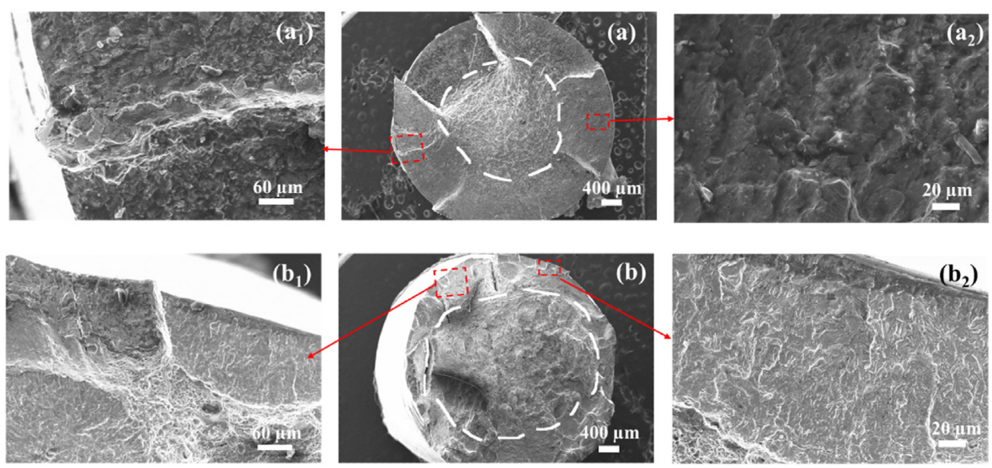


**Fig. 7 – Images taken by SEM of fracture surfaces for the (a) uncharged sample (where $a_1$ and $a_2$ highlight the local region), and (b) hydrogenated sample (where $b_1$ and $b_2$ highlight the local zone).**

respectively. Differences are evident in the: i) characteristic response frequencies, ii) time of crack initiation, and iii) corrosion fatigue life.

As shown in Figs. 3 and 5, the $\Delta p$ peak maximum appears at a specific frequency. This specific frequency can be called 'characteristic response frequency', at which the most obvious change in phase angle is observed. It can be seen from Fig. 8 that in the presence of hydrogen, the characteristic response frequency appears at either 100 Hz or 50 Hz. In an uncharged sample, this occurs at lower frequencies, e.g., 0.1 Hz and 0.01 Hz (Fig. 9). According to the conclusions drawn in Section Theoretical explanation of the phase angle shift in the presence of hydrogen, the presence of hydrogen causes a shorter crack, for which the characteristic response frequency appears at higher frequency than for a longer crack. This offers an explanation as to why the characteristic response frequency in the presence of hydrogen is higher than that in the absence of hydrogen.

The time when a sudden increase appears in the phase shift angle curve can be used to identify the time of crack initiation [31]. As shown in Fig. 8, the crack initiation in the presence of hydrogen appears at around 3 h, while in the absence of hydrogen it appears at approximately 8 h. It is well known that permeated hydrogen accelerates pitting because the passive (or oxide) film on the steel surface is damaged through the interaction with permeated hydrogen [24,37–41]. While crack usually initiates from the pits. Therefore, the crack initiation time in the presence of hydrogen is much shorter than in its absence.

A significant difference in corrosion fatigue life between hydrogenated and uncharged samples is also clearly evident when comparing Figs. 8 and 9. In the absence of hydrogen, the corrosion fatigue life of the sample is around 24 h, which is about two-fold of that of hydrogenated sample. When hydrogen enters the sample, the mechanical properties of the steel, such as tensile strength, hardness and yield strength,

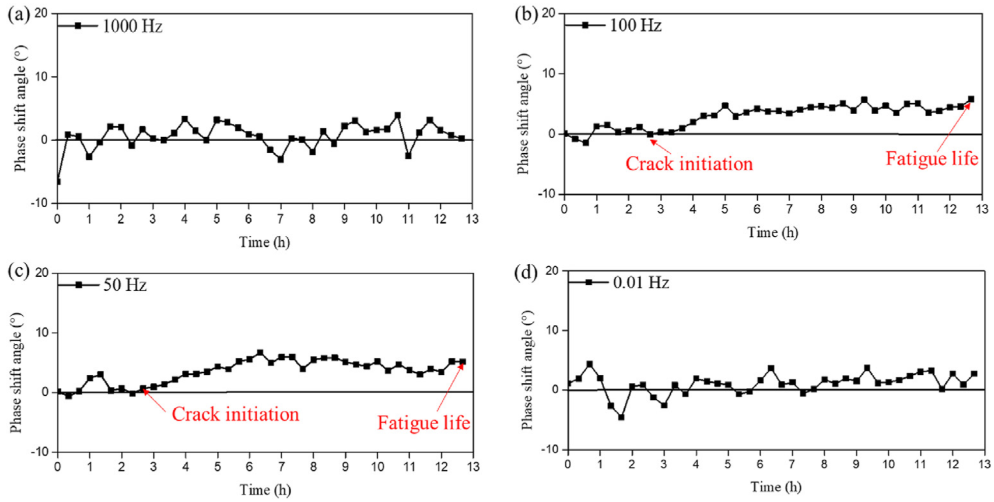


**Fig. 8 – Phase shift angle vs. time curves of a hydrogenated sample at (a) 1000 Hz, (b) 100 Hz, (c) 50 Hz and (d) 0.01 Hz.**

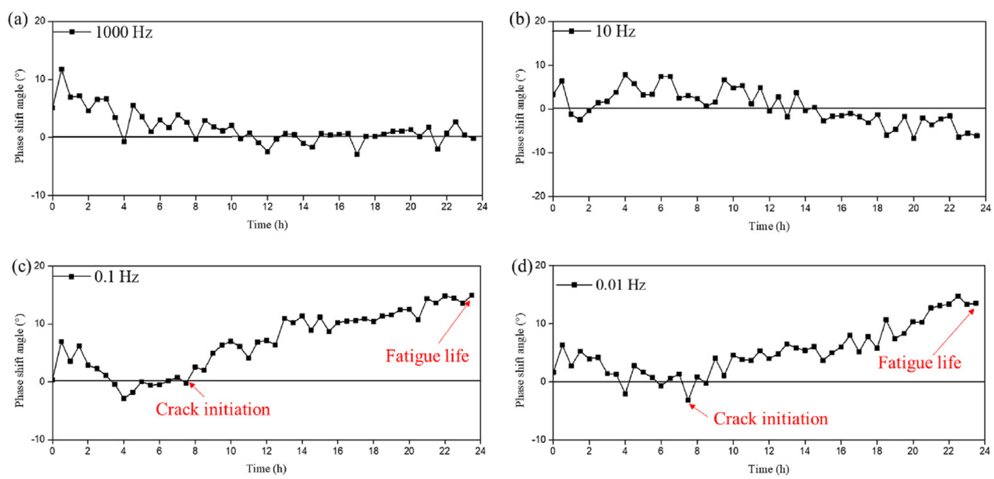


**Fig. 9 – Phase shift angle vs. time curves of an uncharged sample at (a) 1000 Hz, (b) 10 Hz, (c) 0.1 Hz and (d) 0.01 Hz.**

often change. Fig. 7b shows a brittle fracture characteristic of hydrogenated steel sample, indicating that hydrogen degrades the toughness of the steel, hence, the corrosion fatigue life is shortened [42,43].

## Conclusions

The hydrogen effect on EIS Bode plot of the phase angle shift during corrosion fatigue crack emanation in G105 drill pipe steel was investigated. The main conclusions are:

(1) The presence of hydrogen results in a lower peak intensity on the phase angle vs. frequency plot. The peak in the presence of hydrogen is also shifted to higher frequency. These can be attributed to shorter crack length in the presence of hydrogen than in its absence.
(2) Hydrogen shortens both the crack initiation time and the corrosion fatigue life of the G105 drill steel. The former effect is due to enhanced surface pitting resulted from hydrogen, while the latter is due to a decrease in the toughness of the steel following exposure to hydrogen.

## Credit authorship contribution statement

Xiankang Zhong: Methodology, Investigation, Writing - original draft. Yuantai He: Formal analysis, Validation, Investigation. Noam Eliaz: Supervision, Writing - review & editing. Kyra Sedransk Campbell: Writing - review & editing. Junying Hu: Supervision, Funding acquisition.

## Data availability statement

The data that support the findings of this study are available on request from the corresponding author, [J. H.].

## Declaration of competing interest

The authors declare that they have no known competing financial interests or personal relationships that could have appeared to influence the work reported in this paper.

## Acknowledgements

X. Zhong and J. Hu are grateful to the support from the National Natural Science Foundation of China (grant No. 52171080, 51501160) and Scientific and Technological Innovation Team for the Safety of Petroleum Tubular Goods at Southwest Petroleum University (grant No. 2018CXTD01).

## Appendix A. Supplementary data

Supplementary data to this article can be found online at https://doi.org/10.1016/j.ijhydene.2021.09.205.

## REFERENCES

[1] Zamani SM. Failure analysis of drill pipe: a review. Eng Fail Anal 2016;59:605–23. https://doi.org/10.1016/j.engfailanal.2015.10.012.

[2] Lin YH, Lin B, Pan J. Effect of $CO_2$ Corrosion on repeated impact fatigue properties of drill pipe materials. Surf Technol 2019;48:249–55. https://doi.org/10.16490/j.cnki.issn.1001-3660.2019.01.032.

[3] Han Y, Zhao X, Bai Z. Failure analysis on fracture of a S135 drill Pipe. Proce. Mater Sci 2014;3:447–53. https://doi.org/10.1016/j.mspro.2014.06.075.

[4] Chudyk I, Poberezhny L, Hrysanchuk A. Corrosion of drill pipes in high mineralized produced waters. Procedia Struct. Integ 2019;16:260–4. https://doi.org/10.1016/j.prostr.2019.07.050.

[5] Li S, He C, Xu DL. Stress corrosion cracking and corrosion fatigue cracking behavior of A7N01P-T4 aluminum alloy. Mater Corros 2018;69:207–14. https://doi.org/10.1002/maco.201709527.

[6] Luo SJ, Wang R, Zhao K. Effect of dual phase treatment on microstructure and mechanical properties of S135 drill pipe steel. Trans Mater Heat Treat 2013;34:118–22. https://doi.org/10.13289/j.issn.1009-6264.2013.04.024.

[7] Zeng D, Li H, Tian G. Fatigue behavior of high-strength steel S135 under coupling multi-factor in complex environments. Mater Sci Eng 2018;724:385–402. https://doi.org/10.1016/j.msea.2018.03.093.

[8] Li H, Han M. Fatigue and corrosion fatigue behaviors of G105 and S135 high–strength drill pipe steels in air and $H_2S$ environment. Process Saf Environ Protect 2019;124:63–74. https://doi.org/10.1016/j.psep.2019.01.023.

[9] Punpruk S. An effect of pH on corrosion resistance of martensitic and duplex stainless steel in low $H_2S$ environment. Ann Pharmacother 1996;30:1232–4. https://doi.org/10.1177/106002809603001103.

[10] Zhang T, Yao YA, Wei C. Relationship between hydrogen-induced additive stress and threshold cracking stress for a pipeline steel. Acta Metall Sin 2002;38:844–8. https://doi.org/10.1002/mop.10502.

[11] Huang BS, Chen X, Huang LP. Changes of microstructure and properties of G105 drill pipe in $H_2S$ environment. Mater Sci Forum 2015;814:303–12. https://doi.org/10.4028/www.scientific.net/MSF.814.303.

[12] Huang B, Wen X, Li G. Research on impact toughness of 105SS drill pipe in wet $H_2S$ environment. Mater Res Express 2019;6:065508. https://doi.org/10.1088/2053-1591/ab0da1.

[13] Eliaz N, Gileadi E. Physical electrochemistry: fundamentals, techniques, and applications. 2nd ed., 12. Wiley-VCH; 2019. p. 227–322.

[14] Bai P, Zhou J, Luo B, Zheng S, Wang P, Tian Y. Hydrogen embrittlement of X80 pipeline steel in $H_2S$ environment: effect of hydrogen charging time, hydrogen-trapped state and hydrogen charging-releasing-recharging cycles. Int J Miner Metall Mater 2020;27:63–73. https://doi.org/10.1007/s12613-019-1870-1.

[15] Huang F, Cheng P, Zhao XY, Liu J, Hu Q, Cheng YF. Effect of sulfide films formed on X65 steel surface on hydrogen permeation in $H_2S$ environments. Int J Hydrogen Energy 2017;42:4561–70. https://doi.org/10.1016/j.ijhydene.2016.10.130.

[16] Gan L, Huang F, Zhao X, Liu J, Cheng YF. Hydrogen trapping and hydrogen induced cracking of welded X100 pipeline steel in $H_2S$ environments. Int J Hydrogen Energy 2018;43:2293–306. https://doi.org/10.1016/j.ijhydene.2017.11.155.

[17] Lin Y, Li B, Pan J. Effect of $CO_2$ corrosion on repeated impact fatigue properties of drill pipe materials. Surf Technol 2019;48(1):249–55. https://doi.org/10.16490/j.cnki.issn.1001-3660.2019.01.032.

[18] Manigandan K, Srivatsan TS, Quick T. Influence of microstructure and load ratio on cyclic fatigue and final fracture behavior of two high strength steels. Mater Des 2014;55:727–39. https://doi.org/10.1016/j.matdes.2013.10.003.

[19] Han L, Liu M, Luo S, Lu TJ. Fatigue and corrosion fatigue behaviors of G105 and S135 high strength drill pipe steels in air and $H_2S$ environment. Process Saf Environ Protect 2019;124:63–74. https://doi.org/10.1016/j.psep.2019.01.023.

[20] Liu M, Luo S, Shen Y. Corrosion fatigue crack propagation behavior of S135 high strength drill pipe steel in $H_2S$ environment. Eng Fail Anal 2019;97:493–505. https://doi.org/10.1016/j.psep.2019.01.023.

[21] Wan LP, Meng YF, Li G. Corrosion behavior of drilling pipe steels for high sour gas field. Adv Mater Res 2012;415–417:2292–7. https://doi.org/10.4028/www.scientific.net/AMR.415-417.2292.

[22] Zeng D, Tian G, Hu J, Zhang Z, Shi T, Liu W. Effect of immersion time on the mechanical properties of S135 drill pipe immersed in $H_2S$ solution. J Mater Eng Perform 2014;23:4072–81. https://doi.org/10.1007/s11665-014-1198-y.

[23] Zhi Z, Zhou XY, Zeng DZ, Zhang JY, Shi T. Evaluation on chloride cracking of S135 high-strength drill pipe. Adv Mater Res 2012;430–432:636–9. 0.4028/www.Scific.net/AMR.430-432.636.

[24] Rajabipour A, Melchers RE. Service life of corrosion pitted pipes subject to fatigue loading and hydrogen embrittlement. Int J Hydrogen Energy 2018;43:844–8450. https://doi.org/10.1016/j.ijhydene.2018.03.063.

[25] Gao Z, Gong B, Xu Q, Wang D, Deng C, Yu Y. High cycle fatigue behaviors of API X65 pipeline steel welded joints in air and $H_2S$ solution environment. Int J Hydrogen Energy 2021;46:10423–37. https://doi.org/10.1016/j.ijhydene.2020.12.140.

[26] Dadfrnia M, Sofronis P, Brouwer J, Sosa S. Assessment of resistance to fatigue crack growth of natural gas line pipe steels carrying gas mixed with hydrogen. Int J Hydrogen Energy 2019;44:10808–22. https://doi.org/10.1016/j.ijhydene.2019.02.216.

[27] An T, Peng H, Bai P, Zheng S, Wen X, Zhang L. Influence of hydrogen pressure on fatigue properties of X80 pipeline steel. Int J Hydrogen Energy 2017;42:15669–78. https://doi.org/10.1016/j.ijhydene.2017.05.047.

[28] Bosch RW. Electrochemical impedance spectroscopy for the detection of stress corrosion cracks in aqueous corrosion systems at ambient and high temperature. Corrosion Sci 2005;47:125–43. https://doi.org/10.1016/j.corsci.2004.05.018.

[29] Bosch RW, Moons F, Zheng JH, Bogaerts WF. Application of electrochemical impedance spectroscopy for monitoring

stress corrosion cracking. Corrosion 2001;57:532–9. https://doi.org/10.1016/S0950-0618(01)00002-2.
[30] Luo X, Singh PM. Phase angle analysis for stress corrosion cracking of carbon steel in fuel-grade ethanol: experiments and simulation. Electrochim Acta 2010;56:1835–47. https://doi.org/10.1016/j.electacta.2010.07.024.
[31] He Y, Zhong X, Hu J, Hou D, Zhang Z, Zeng DZ, Shi T. Monitoring corrosion fatigue drack formation on drill steel using electrochemical impedance spectroscopy: experiment and modeling. Corrosion Sci 2020;175:108880. https://doi.org/10.1016/j.corsci.2020.108880.
[32] Navi NU, Tenenbaum J, Sabatani E, Kimmel G, David RB, Rosen BA, Barkay Z, Ezersky V, Tiferet E, Ganor YI, Eliaz N. Hydrogen effects on electrochemically charged additive manufactured by electron beam melting (EBM) and wrought Ti–6Al–4V alloys. Int J Hydrogen Energy 2018;45:25523–40. https://doi.org/10.1016/j.ijhydene.2020.06.277.
[33] Zhong X, Schulz M, Wu CH, Rabe M, Erbe A, Rohwerder M. Limiting current density of oxygen reduction under ultrathin electrolyte layers: from the micrometer range to monolayers. ChemElectroChem 2021;8:712–8. https://doi.org/10.1002/celc.202100083.
[34] Kovač J, Kosec T, Legat A. Monitoring behavior of 304 stainless steel under constant tensile loading by electrochemical impedance spectroscopy. Corrosion Eng Sci Technol 2012;47:478–83. https://doi.org/10.1179/1743278212y.0000000029.
[35] Trethewey KR, Paton M. Electrochemical impedance behavior of type 304L stainless steel under tensile loading. Mater Lett 2004;58(27/28):3381–4. https://doi.org/10.1016/j.matlet.2004.02.048.
[36] Luo H, Dong CF, Liu ZY. Characterization of hydrogen charged of 2205 duplex stainless steel and its correlation with hydrogen-induced cracking. Mater Corros 2013;64:26–33. https://doi.org/10.1002/maco.201106146.
[37] Li J, Zhong X, Wang T, Hu JY, Zhang Z, Zeng DZ, Shi T. Synergistic effect of erosion and hydrogen on properties of passive film on 2205 duplex stainless steel. J Mater Sci Technol 2021;67:1–10. https://doi.org/10.1016/j.jmst.2020.08.004.
[38] Guo LQ, Qin XQ, Yang BJ. Effect of hydrogen on semiconductive properties of passive film on ferrite and austenite phases in a duplex stainless steel. Sci Rep 2017;7:3317. https://doi.org/10.1038/s41598-017-03480-8.
[39] Michalska J. The effect of hydrogen on pitting corrosion of superaustenitic and austenitic-ferritic stainless steels. 10.4028/www.Scific.net/DDF Defect Diffusion Forum 2012;326–328:620–5.
[40] Wei R, Chen X, Ai Z, Jin Y. Experimental study and numerical simulation on SSCC in FV 520B stainless steel exposed to $H_2S+Cl^-$ environment. Int J Hydrogen Energy 2018;42:9059–67. https://doi.org/10.1016/j.ijhydene.2018.03.119.
[41] Yang ZX, Li JX, Su YJ, Qiao LJ. Hydrostatic pressure effects on stress corrosion cracking of X70 pipeline steel in a simulated deep-sea environment. Int J Hydrogen Energy 2017;44:27446–57. https://doi.org/10.1016/j.ijhydene.2017.09.061.
[42] Eliaz N, Shachar A, Tal B, Eliezer D. Characteristics of hydrogen embrittlement, stress corrosion cracking and tempered martensite embrittlement in high-strength steels. Eng Fail Anal 2002;9:167–84. https://doi.org/10.1016/S1350-6307(01)00009-7.
[43] Singh V, Singh R, Arora KS, Mahajan KD. Hydrogen induced blister cracking and mechanical failure in X65 pipeline steels. Int J Hydrogen Energy 2019;39:22039–49. https://doi.org/10.1016/j.ijhydene.2019.06.098.